Computational Design of Metal Hydrides on a Defective Metal–Organic Framework HKUST-1 for Ethylene Dimerization

Karam Hashem,[a,b] Ramakrishna Krishnan,[a] Kuiwei Yang,[a] Bai Amutha Anjali,[a] Yugen Zhang,[b] and Jianwen Jiang[a]*

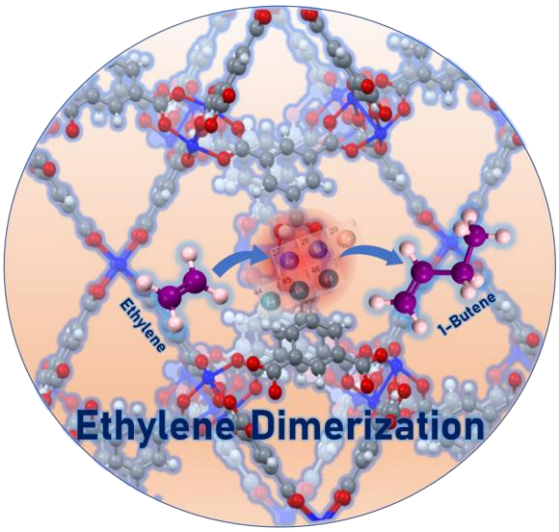
[a]*Department of Chemical and Biomolecular Engineering, National University of Singapore, 117576, Singapore*
[b]*Institute of Sustainability for chemicals, Energy and Environment (ISCE2), Agency for Science, Technology and Research (A*STAR), 1 Pasek Road Jurong Island, Singapore 627833, Republic of Singapore*

Abstract: Catalytic ethylene dimerization to 1-butene is a crucial reaction in the polymer industry, as 1-butene is used in the production of most common plastics (linear low-density and high-density polyethylene). With well-defined tunable structures and unsaturated active sites, defective metal–organic frameworks have recently emerged as potential catalysts for ethylene dimerization. Herein, we computationally design a series of metal hydrides on defective HKUST-1 namely H-M-DHKUST-1 (M: Co, Ni, Cu, Ru, Rh and Pd), subsequently assess their catalytic activity for ethylene dimerization by density functional theory calculations. Due to the antiferromagnetic behavior of the dimeric metal-based clusters, we comprehensively investigate all possible multiplicity states on H-M-DHKUST-1 and multiplicity crossing is observed. The ground-state reaction barriers for the four elementary steps involved in ethylene dimerization are rationalized and C-C coupling is revealed to be the rate-determining step on H-Co-, H-Ni-, H-Ru-, H-Rh-, and H-Pd-DHKUST-1. The energy barrier for β-hydride elimination is found to be the lowest on H-Ru- and H-Rh-DHKUST-1, as attributed to weak stability of agostic arrangement; however, the energy barrier for 1-butene desorption is the highest on H-Rh-DHKUST-1. Among the designed H-M-DHKUST-1, Co- and Ni-based are predicted to possess the best overall catalytic performance. The mechanistic insights from this study may facilitate the development of new MOFs towards efficient ethylene dimerization and other industrially important reactions.

Keywords: Defective metal–organic frameworks, hydrides, ethylene dimerization, 1-butene, density functional theory

*Email: chejj@nus.edu.sg

Graphical abstract



1. Introduction

Light olefins are the primary feedstock of many petrochemical and refinery processes with annual production of over 160 million tons.[1] Particularly, ethylene receives the major focus in steam cracking plants and accounts for ~40% of the global market of light olefins.[2] In the last decade, ethylene transformation into more valuable products like linear alpha olefins (LAO) has increased considerably from 7 million metric tons per year (Mtpy) in 2016 to more than 8.5 Mtpy in 2021. Ethylene dimerization into 1-butene is a key process in the production of polyethylene, as 1-butene is used to produce common plastics, e.g., linear low-density polyethylene (LLDPE) and high-density polyethylene (HDPE). Commercially, ethylene dimerization to 1-butene is achieved on homogenous catalysts in the presence of aluminium activators.[3-6] These homogeneous Ziegler-Natta catalysts are highly selective, but lack recyclability and require environmentally undesirable solvents and activators. While heterogeneous catalysts like metal oxides are also explored for this reaction, they exhibit low selectivity and yield.[7-9] Therefore, it is highly desired to develop robust catalysts for effective ethylene dimerization to 1-butene.

Metal–organic frameworks (MOFs) are a class of hybrid nanoporous materials, in which metal clusters are assembled with organic ligands to form extended networks.[10] With readily tuneable structures and functionalities, MOFs possess an unprecedentedly large degree of design flexibility from diverse metal and organic building blocks. These salient features have attracted considerable interest in using MOFs for many potentials applications. In MOFs, organic linkers or metal nodes can be truncated, thus producing defective MOFs (DMOFs) with multiple pore sizes and/or vacancies. Generally, there are two procedures to synthesize DMOFs: *de novo* method by truncating linkers during synthesis and post-synthetic modification of pristine MOFs to eliminate chemisorbed coordination modulators.[11] Common DMOFs include HKUST-1,[12, 13] MOF-5,[14] UiO-66,[15, 16] and MIL-101.[17-19]

With readily accessible open metal sites as well as rich electronic configuration and structural environment, DMOFs have demonstrated high potential in selective ethylene dimerization and oligomerization.[20] Using mixed ligand approach, Fischer and coworkers introduced defects into Ru-HKUST-1 with one linker (benzene-1,3,5-tricarboxylate) replaced by pyridine-3,5-dicarboxylate, generating coordinatively unsaturated metal sites; then tested the catalytic activity for ethylene dimerization in toluene with the presence of Et_2AlCl at 80 °C and 55 bar.[21] A long-term stability over 24 h was observed, despite a low catalytic activity with turnover frequency (TOF) of 4.36 h^{-1}. Nevertheless, the catalytic activity in a liquid phase was

enhanced by increasing the concentration of defective metal sites in Ru-HKUST-1.[22] They also synthesized defective monometallic Ru-HKUST-1 (univalent Ru^{II}-Ru^{II} and multivalent Ru^{II}-Ru^{III}), Rh-HKUST-1 and bimetallic Ru/Rh-HKUST-1 by controlling the formation of defects through thermal elimination and/or fragmentation of organic ligands to generate highly accessible unsaturated metal sites of reduced oxidation states.[23] Subsequently, Soukri and coworkers created two types of defects in Ru-HKUST-1 and examined their effects on ethylene dimerization and 1-butene selectivity.[24] The defective Ru-HKUST-1 was synthesized via incorporating 25% of pyridine-3,5-dicarboxylate ligands in hydrogen gas at 150 ºC. This led to the formation of highly accessible and robust Ru-H species for ethylene dimerization due to heterolytic H-H bond breaking. After pre-treatment in N_2 gas at 200 ºC, ethylene dimerization was tested in H_2 at 4.2 MPa and 150 ºC. The defective Ru-HKUST-1 showed high selectivity (99%) and stability (> 120 h) with TOF > 200 h^{-1} in optimal conditions. Meanwhile, from density-functional theory (DFT) calculations, they found similar electronic energy profiles for ligand- and thermal-engineered defective Ru-HKUST-1 following the Cossee-Arlman mechanism.[25] The rate-determining step was predicted to be C-C coupling with energy barriers of 20.9 and 21.4 kcal/mol on the ligand- and thermal-engineered defective Ru-HKUST-1, respectively. Furthermore, the activation of β-hydride was found to barrierless, the adsorption of ethylene and desorption of 1-butene were predicted with barriers of 6.7 and 26 kcal/mol, respectively.[24]

While the above handful of studies have demonstrated the catalytic activity of DMOFs for ethylene dimerization, extremely pure 1-butene (99.7%) is required for polyethylene production.[26, 27] To develop stable, sustainable and economic catalysts with reasonable activity and high 1-butene selectivity, it is indispensable to better understand the mechanism of ethylene dimerization from bottom-up. In this context, computation at the electronic structure level is crucial as it is capable of predicting catalytic activity and selectivity, identifying preferential reaction pathway and probable products. Such microscopic insights would facilitate designing and tunning high-performance catalysts.

In this study, we computationally design a series of metal hydrides on defective HKUST-1 (H-M-DHKUST-1, M: metal atom), then evaluate their catalytic performance for ethylene dimerization through DFT calculations. As shown in **Figure S1**, the metals include late transition metals of 3d and 4d, specifically Co, Ni, Cu, Ru, Rh and Pd, because these metals usually exhibit considerable activity for ethylene dimerization via the Cossee-Arlman route.[19] Our motivation is to mechanistically understand ethylene dimerization on H-M-DHKUST-1,

including the effects of multiplicity, electronic configuration and structural environment. By comparing the performance of different H-M-DHKUST-1, we can identify which metal is the best and possibly design new H-M-DHKUST-1 with low-cost metals for ethylene dimerization and other catalytic reactions.

2. Methodology

HKUST-1 consists of a paddle-wheel like secondary building unit (SBU), in which four 1,3,5-benzene tricarboxylate (BTC) linkers are bridged with dimeric Cu atoms (**Figure 1a**).[28] Defective HKUST-1 (DHKUST-1) is created when one BTC linker is missing, as shown in **Figure 1b** for its cluster model with cleaved bonds saturated by -CN groups. DHKUST-1 can be experimentally activated by thermal treatment in H_2 atmosphere (**Figure 1c**) to produce monohydride DHKUST-1 (**Figure 1d**).[11, 21, 24] To investigate the effect of metal, the Cu atoms can be replaced by different metals.[21]

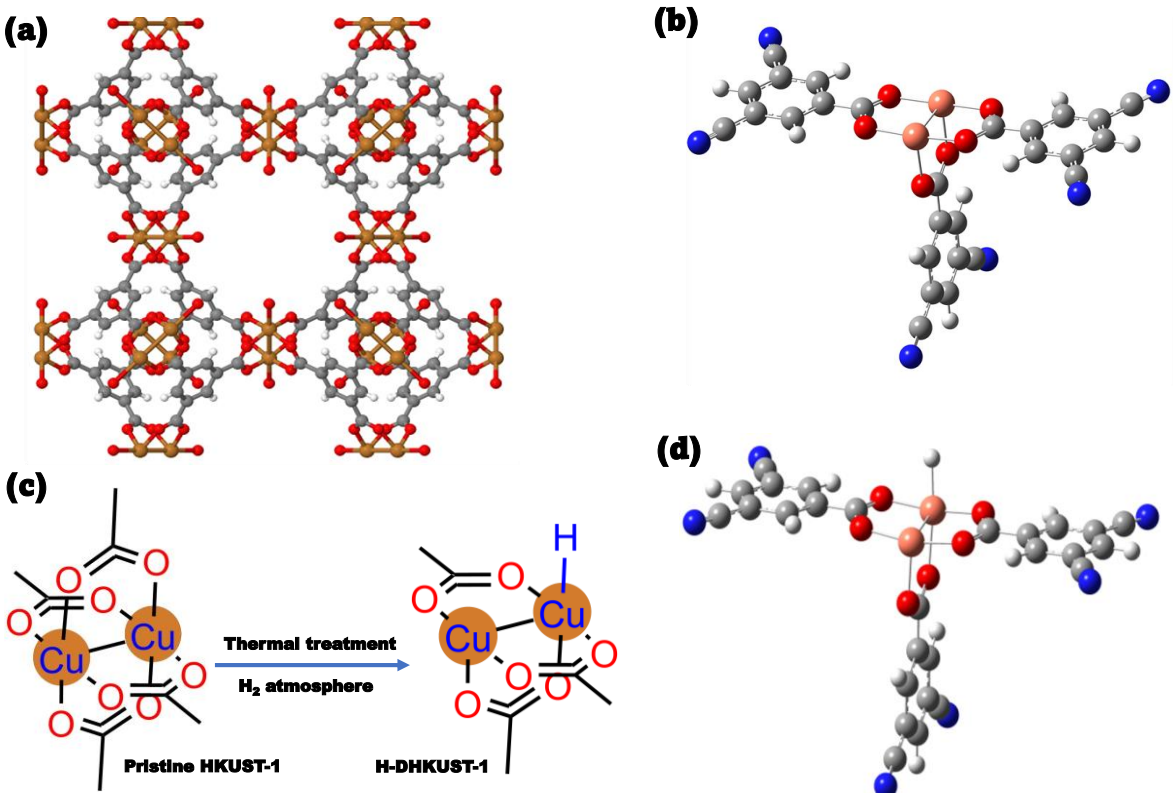


Figure 1. (a) Crystal structure of HKUST-1. (b) Cluster model of DHKUST-1. (c) Activation of DHKUST-1 to monohydride DHKUST-1 shown in (d). Copper, nitrogen, carbon, oxygen, and hydrogen atoms are in brown, blue, grey, red, and white, respectively.

We consider six monohydrides H-M-DHKUST-1 with M = Co, Ni, Cu, Ru, Rh and Pd. Simplified as the cluster models, all the H-M-DHKUST-1 were optimized using M06-L functional, which performs well for transition metals and accounts for medium-range dispersion interactions.[29] The polarized split-valence basis set def2-SVP[30] was used for p-block atoms (H, C, N and O atoms), and the doubly polarized triple-ζ basis set def2-TZVPP were used for 3d and 4d metals.[29, 30] The built-in effective core potential in def2-TZVPP was also applied for 4d metals. The nitrogen atoms in -CN were fixed during optimization. Due to the formation of long-range magnetic electron spin ordering with conjugated linkers, MOFs with dimeric transition metals were found to exhibit antiferromagnetic behavior.[31-33] Thus, stability calculations were performed to identify the stable electronic configurations of H-M-DHKUST-1. Thereafter, vibrational frequencies were computed at the same level of theory to verify the nature of stationary points (no imaginary frequency for an energy minimum and only one imaginary frequency for a transition state) and provide thermal corrections to thermochemical properties. Each transition state was confirmed to directly connect with reactant and product through the intrinsic reaction coordinate (IRC) calculations. The reaction pathway of ethylene dimerization based on the Cossee-Arlman route was examined by considering all reasonable multiplicities to deduce the ground-state intermediates and transition states. To further understand the charges of catalytic sites and charge transfer during reaction, the Natural Bond Orbital (NBO) charges were evaluated at the same level of theory. The Gibbs energies (G) were estimated at 298.15 K by $G = E + G_{corr,}$ where E is the electronic energy and G_{corr} is the thermal correction. All the calculations were performed with Gaussian 16 package.[34] The relative Gibbs energy profiles ΔG were constructed by combining all key intermediates and transition states. Moreover, possible intersystem spin crossing (ISC) was explored from the energy profiles and its effect was quantified.

3. Results and Discussion

We first present the stable electronic configurations and NBO charges on six H-M-DHKUST-1 clusters (M: Co, Ni, Cu, Ru, Rh and Pd) clusters, as well as the M-H and M-M bond lengths. Then, relative Gibbs energy profiles for four elementary steps (initiation, C-C coupling, β-hydride elimination, and 1-butene desorption) are closely examined and the Gibbs energy barriers are quantified, thus predicting the favourable/unfavourable steps. Furthermore, the catalytic activity of H-M-DHKUST-1 is compared with other MOFs reported in the literature, including MFU-4*l*(Ni), Ni, Co, Cu and Pd-decorated NU-1000.[35-38] Finally, the

effects of multiplicity on stability and Gibbs energy are discussed for electronic-structural intercorrelations in different intermediates and transition states.

3.1. Stability and NBO charges

As listed in **Tables S1–S7**, the open-shell electronic configurations are stable on Co, Ni, Ru and Pd based H-M-DHKUST-1 clusters, while the closed-shell configurations are stable on Cu and Rh based clusters. Quintet is the ground-state multiplicity on H-Co-DHKUST-1, triplet on H-Ni-DHKUST-1 and H-Ru-DHKUST-1, open-shell singlet on H-Pd-DHKUST-1, and closed-shell singlet on H-Cu-DHKUST-1 and H-Rh-DHKUST-1, respectively. The electronic energies at different multiplicities are also provided, as well as the energy differences relative to the ground-state multiplicity. **Figure 2** shows the optimized structures with M-H bond lengths on the six H-M-DHKUST-1 clusters. There is a bridged hydride between the dimeric Cu atoms on H-Cu-DHKUST-1, and this hydride is not centered between the two Cu atoms but shifted to one of them giving partial hetero-valent arrangement of Cu-H-Cu. On the other five H-M-DHKUST-1 clusters, a vertically bonded hydride on one metal is observed and causes apparent hetero-valent configuration of dimeric metals. This information introduces a prior knowledge in the accessibility of hydride for initiating ethylene dimerization.

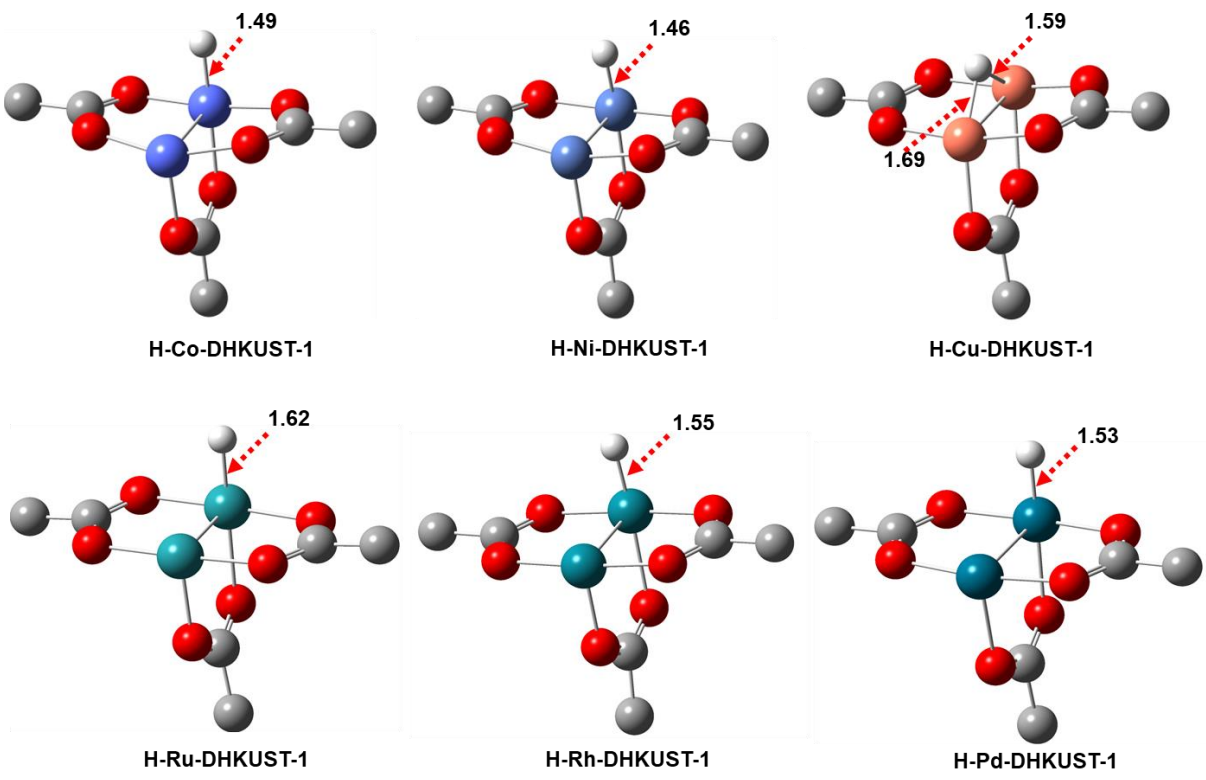
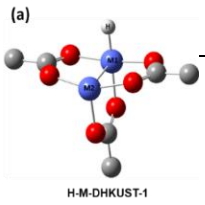


Figure 2. Optimized structures with M-H bond lengths (Å) on H-M-DHKUST-1. Carbon, oxygen and hydrogen atoms are in grey, red and white, respectively.

Table 1 lists the M-H and M-M bond distances on the six H-M-DHKUST-1 clusters. The M-H bond length increases in the order of H-Ni-DHKUST-1 < H-Co-DHKUST-1< H-Pd-DHKUST-1 < H-Rh-DHKUST-1 < H-Cu-DHKUST-1 < H-Ru-DHKUST-1. The longest M-H bond distance is 1.62 Å on H-Ru-DHKUST-1, which implies that this cluster is the most readily accessible among the six for hydride-based reaction. Also listed in **Table 1** are the NBO charges on H and M atoms. The NBO charges of the hydride H atoms on metals are nearly zero, which was also observed in β-hydride elimination on Au(III) products[39] and metal complexes.[40, 41] This phenomenon is attributed to the high electronegativity of oxygen atoms surrounding metals; consequently, the charges are redistributed within the cluster. From Bent's rule, increasing ionic character of M-O bond would lead to decreasing *d*-character of M-H bond.[42] Due to the high electronegativity of oxygen, the M-O bond is expected to attain high *d*-character, corresponding to the low *d*-character of M-H bond and the small negative charge of hydride H atom. It is also noticed that 4d metals attached to hydride carry smaller NBO charges than the corresponding 3d metals, while the secondary metal atoms hold larger NBO charges. Specifically, Rh and Ru have the smallest charges of 0.363*e* and 0.435*e*, respectively. The stabilization of hydride on metal and its availability for initiating ethylene dimerization are expected to depend on the type of metal.

Table 1. M-H and M-M bond distances (Å), NBO charges (in terms of *e*) of H and M atoms on H-M-DHKUST-1. (a) vertical hydride and (b) bridged hydride.



H-M-DHKUST-1	ℓ_{M1-H}	ℓ_{M2-H}	ℓ_{M1-M2}	Q_H	Q_{M1}	Q_{M2}
H-Co-DHKUST-1(q)	1.49	2.905	2.45	0.001	0.537	0.985
H-Ni-DHKUST-1(t)	1.46	2.577	2.33	0.003	0.507	0.986
H-Cu-DHKUST-1(cs)	1.59	1.692	2.41	-0.053	0.786	0.800
H-Ru-DHKUST-1(q)	1.62	2.791	2.25	0.001	0.435	0.873
H-Rh-DHKUST-1(cs)	1.55	2.910	2.40	0.047	0.363	0.808
H-Pd-DHKUST-1(t)	1.53	3.020	2.54	0.088	0.473	0.815

To predict catalytic properties and design efficient catalysts, it is indispensable to understand the oxidation state and coordination environment of metallic dimer on H-M-DHKUST-1. **Tables S8-S13** list the optimized M-M bond distances (Å), NBO charges, and NBO spin density distributions in ground-state intermediates and transition states. On the bimetallic sites, the metallic interaction can significantly affect multiplicity, which is directly

related to the number of unpaired electrons, and this interaction can cause a change in electronic configuration, as reported on perfect HKUST-1 and bimetallic paddlewheel complexes.[43-45] Clusters with open shell configurations such as quintet on H-Co-DHKUST-1 and H-Ru-DHKUST-1, as well as triplet on H-Ni-DHKUST-1 and Pd-DHKUST-1, tend to possess an oxidation state of +2 on both metal atoms. The formation of M-M bond in each metallic dimer consumes one unpaired electron from each metal atom, with remaining two, two, one and one unpaired electrons in each metal atom on H-Co-, H-Ru-, H-Ni- and H-Pd-DHKUST-1 clusters, respectively. Due to difference in coordination environment, the electron spin density in the secondary metal atom is found to be larger than in the primary counterpart. Specifically, the electron spin densities are Co_2 = 2.351*e*, Ru_2 = 2.374*e*, Ni_2 = 1.432*e* and Pd_2 = 1.166*e*; by contrast Co_1 = 1.514*e*, Ru_1 = 1.428*e,* Ni_1 = 0.427*e* and Pd_1 = 0.395*e*. We thus infer there is electron delocalization from the primary to secondary metal atom. However, the closed-shell singlet configuration on H-Cu-DHKUST-1 and H-Rh-DHKUST-1 suggests a complete filled suborbital in each metal atom, where no unpaired electrons exist. It is likely that each metal atom is divalent like $Cu^{2+}(d^9)$ and $Rh^{2+}(d^7)$, and the two unpaired electrons from each atom interact to form M-M bond. An alternative is the formation of multivalent metal dimer $Cu_1^{+}(d^{10})$–$Cu_2^{3+}(d^8)$ and $Rh_1^{+}(d^8)$–$Rh_2^{3+}(d^6)$. Overall, the approximate determination of oxidation state from NBO electron density distribution provides valuable insight into the electronic structure and coordination environment of a catalyst, which is essential for understanding its catalytic activity.

3.2. Catalytic mechanism and activity

Ethylene dimerization catalysed by defective Ru-HKUST-1 and other similar MOFs were revealed to follow the Cossee-Arlman mechanism.[24, 46] We also consider this mechanism in the current study on H-M-DHKUST-1. As shown in **Figure 3**, there are four elementary steps, namely initiation, C-C coupling, β-hydride elimination, and 1-butene desorption. (1) initiation starts with an ethylene molecule adsorbed on catalyst **1** to form a complex **2**, which is then hydrogenated to ethyl intermediate **3**; (2) upon supplying another ethylene molecule to form intermediate **4**, M-ethyl bond breaks and C-C coupling occurs to generate butyl intermediate **5**; (3) after reorientation of butyl intermediate **5** to form **6**, β-hydride elimination takes pace to form intermediate **7** with 1-butene adsorbed; (4) the final step is 1-butene desorption and catalyst **1** is recovered. The reaction cycle can be restored with successive supply of ethylene.

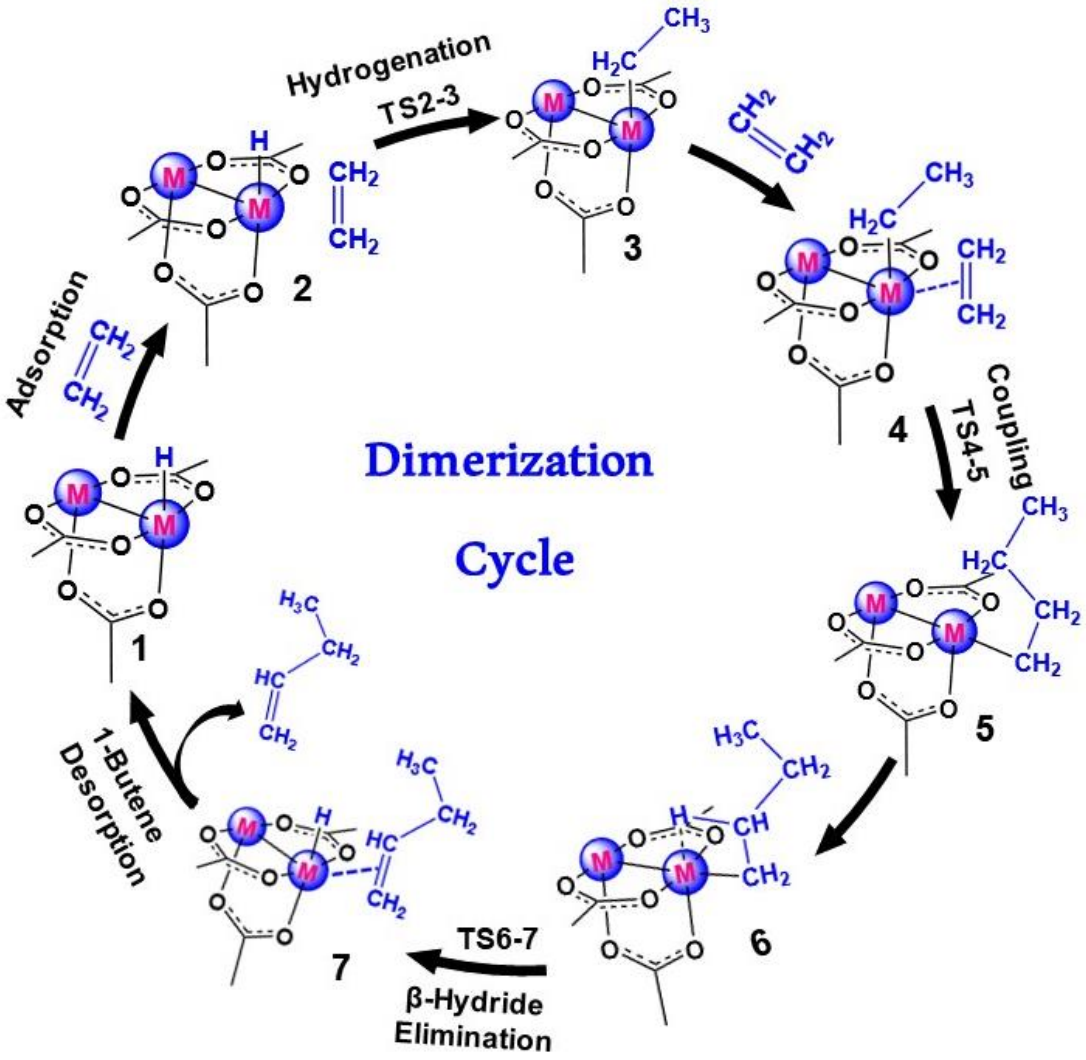


Figure 3. Ethylene dimerization to 1-butene via the Cossee-Arlman mechanism with four elementary steps: initiation (including adsorption and hydrogenation), C-C coupling, β-hydride elimination, and 1-butene desorption.

To identify the ground-state configurations of intermediates and transition states during ethylene dimerization, we performed a deep analysis of relative Gibbs energies Δ*G* at different multiplicities on H-M-DHKUST-1 clusters (**Tables S14-S19** and **Figures S2–S7**). The effects of multiplicity on energy will be discussed in detail below (Section 3.3). **Table S20** lists the imaginary frequencies of transition states for hydrogenation, C-C coupling and β-hydride elimination. Single imaginary frequency is observed for each transition state, which confirms the nature of each stationary point. Since the stable configurations on H-Cu-DHKUST-1 and H-Rh-DHKUST-1 are closed-shell, stability analysis was further conducted for ethylene dimerization on these two clusters (**Table S7**). Stability calculation of the closed shell singlet on H-Rh-DHKUST-1 reveals that the stable closed-shell configurations are maintained throughout all the intermediates and transition states, while the stable open-shell configurations

are observed for species **2**, **TS2-3**, **TS4-5**, **TS6-7** and **7** on H-Cu-DHKUST-1. This finding implies that the electronic structures of intermediates and transition states on the two clusters are substantially different, which would likely cause the two clusters to display different electronic configurations for the reaction. **Figure 4** summarize the Δ*G* profiles of ethylene dimerization on the six H-M-DHKUST-1 (M: Co, Ni, Cu, Ru, Rh, Pd). The profiles include four elementary steps for ethylene dimerization: initiation (adsorption and hydrogenation), C-C coupling, β-hydride elimination, and 1-butene desorption.

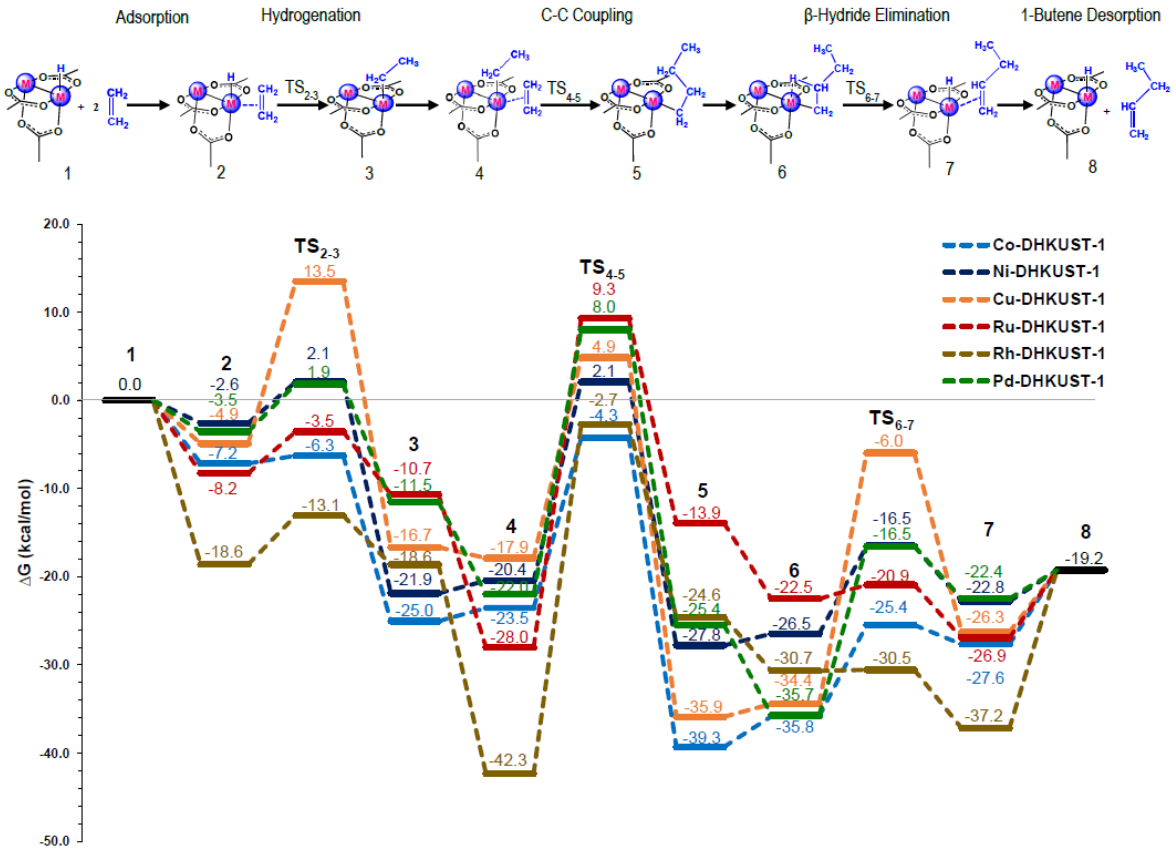


Figure 4. Δ*G* profiles of ethylene dimerization on H-M-DHKUST-1. The top illustrates the four elementary steps: initiation (adsorption and hydrogenation), C-C coupling, β-hydride elimination, and 1-butene desorption. The Gibbs energy barriers G_b are listed in **Table 2**.

Initiation: Initiation includes ethylene adsorption and hydrogenation. Ethylene adsorption is accompanied with a decrease in Gibbs energy. As shown in **Figure 5** for the optimized structures of intermediate **2**, the M-H bonds increase to 1.61, 1.61, 1.72 Å on H-Co-, H-Ni-, H-Cu-DHKUST-1 upon ethylene adsorption from 1.49, 1.46, 1.59 Å (**Figure 2**). On H-Ru-, H-Rh-, H-Pd-DHKUST-1, however, the bonds remain nearly unchanged. Geometry analysis of intermediate **2** suggests two potential hydride modes. These modes are crucial in determining

the extent to which the hydride is accessible for transforming π-complex into alkyl form on H-M-DHKUST-1. The 3d metal-based clusters (H-Co, H-Ni-, and H-Cu-DHKUST-1) adsorb ethylene in a bridged hydride mode, with the hydride approaching to the secondary metal as on the pristine H-Cu-DHKUST-1. The M-H bond lengths are 1.61 and 1.81 Å on H-Co-DHKUST-1, 1.61 and 1.63 Å on H-Ni-DHKUST-1. Such hydrides bridged between M-M sites with long M-H bond lengths would not hinder ethylene hydrogenation on these two clusters. On H-Cu-DHKUST-1, however, the hydride is likely being less accessible because one of M-H bond lengths is only 1.57 Å. On 4d metal-based clusters (H-Ru, H-Rh-, and H-Pd-DHKUST-1), the primary metal adsorbs ethylene with no interference from the secondary metal; their M-H bond lengths are 1.61, 1.55, and 1.53 Å. Upon adsorption, shorter distancing is noticed between the C atom of adsorbed ethylene and the metal atom on H-Ni-DHKUST-1 (2.13 Å) and H-Rh-DHKUST-1 (2.17 Å), compared to the other four clusters. The shorter bridged hydride (i.e., M-H bond) and shorter distancing of ethylene-metal facilitate ethylene adsorption. Consequently, the adsorption of ethylene on H-Rh-DHKUST-1 exhibits an energy decrease of 18.6 kcal/mol, which is the most favorable among the six clusters. While the M-H bonds are altered upon ethylene adsorption, the M-M bonds are also affected. Compared to the pristine clusters, as listed in **Tables S8-S13**, ethylene adsorption induces spin transition on H-Ni-DHKUST-1 (from triplet to open-shell singlet) and H-Cu- DHKUST-1 (from closed-shell to open-shell singlet), accompanied by minor NBO charge distributions. In contrast, the primary metal atoms on Co-, and Ru- and Rh- clusters become significantly more anionic upon interaction with C=C in ethylene. Moreover, the M-M bonds are shorter on H-Co-DHKUST-1 (2.37 Å), elongated on H-Ni- (2.58 Å), H-Cu- (2.48 Å), H-Ru- (2.32 Å) and H-Rh-DHKUST-1 (2.47 Å), and unchanged on H-Pd-DHKUST-1 (2.56 Å).

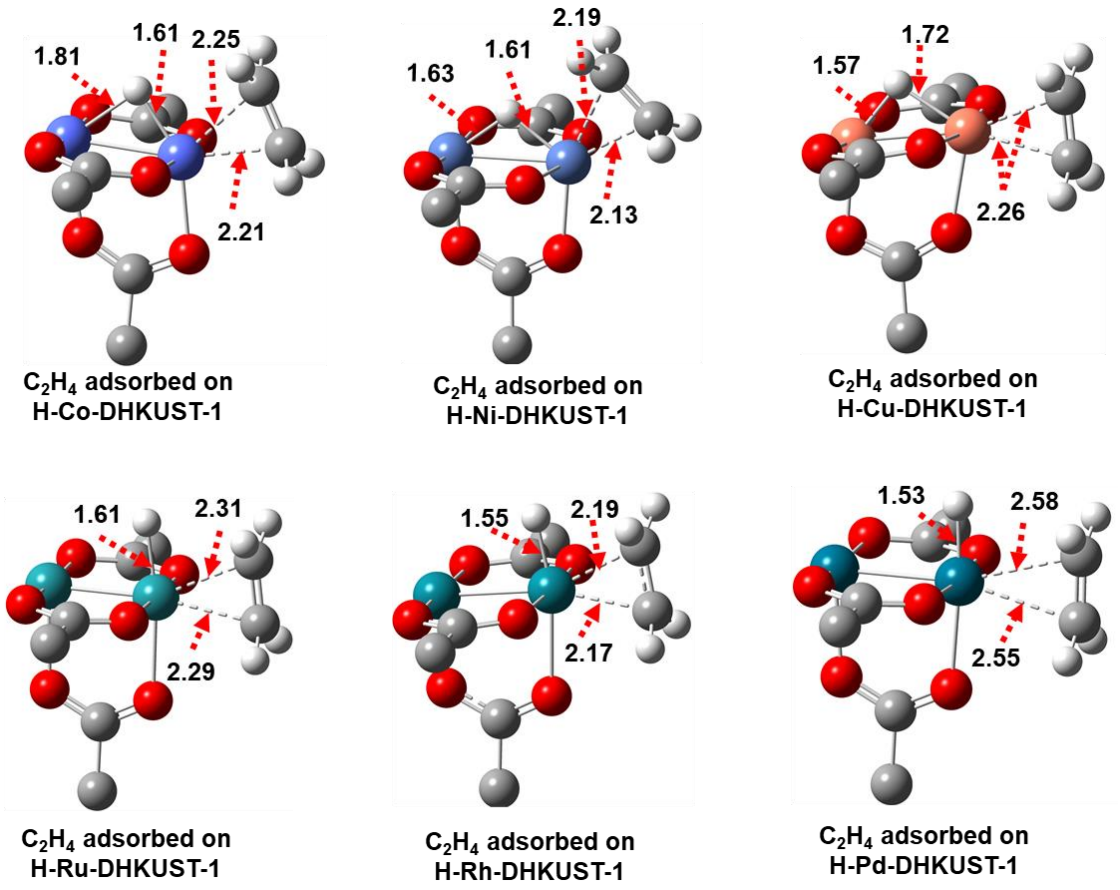


Figure 5. Optimized structures and key bond distances (Å) of intermediate **2** for ethylene adsorption on H-M-DHKUST-1. Carbon, oxygen and hydrogen atoms are in grey, red and white, respectively.

When hydrogenation occurs, the M-H bonds of transitions state **TS2-3** are observed in **Figure S8** to become shorter from intermediate **2** on H-Co- (1.48 Å) and H-Ni-DHKUST-1 (1.47 Å), longer on H-Cu-DHKUST-1 (1.83 Å), and remain nearly the same on the other three clusters. Meanwhile, the M-M bonds become longer as listed in **Tables S8-S13** on H-Co- (2.46 Å), H-Ru (2.40 Å) and H-Rh-DHKUST-1 (2.64 Å) from intermediate **2**, largely unchanged on H-Cu- (2.50 Å) and H-Pd-DHKUST-1 (2.59 Å), but shorter on H-Ni-DHKUST-1 (2.41 Å). **Table 2** lists the Gibbs energy barriers G_b for hydrogenation on the six H-M-DHKUST-1. The G_b are 0.9, 4.7, 4.7, 5.5, and 5.4 kcal/mol on Co, Ni, Ru, Rh and Pd-based clusters, respectively, whereas the G_b on H-Cu-DHKUST-1 is significantly higher with a value of 18.4 kcal/mol. This is consistent with the less accessible hydride on H-Cu-DHKUST-1, in which one of M-H bond lengths is only 1.57 Å. Overall, for the initiation step including both adsorption and hydrogenation, the largest change in M-M bond length is observed on H-Ru- and H-Rh-DHKUST-1 from 2.25 to 2.40 Å and 2.40 to 2.64 Å, respectively. Thus, H-Ru- and H-Rh-

DHKUST-1 possess a greater tolerance than the other four clusters in terms of structural change. On H-Co- and H-Ni-DHKUST-1, the M-M bond lengths are restored to a certain extent due to multiplicity transitions. Specifically, on H-Co-DHKUST-1, the multiplicity is initially quintet intermediate **2** then to triplet in **TS2-3**; the M-M bond length changes from 2.45 to 2.37 then to 2.46 Å. On H-Ni-DHKUST-1, the M-M bond length changes from 2.33 to 2.58 then to 2.41 Å upon multiplicity transition from triplet to open-shell singlet then back to triplet.

Table 2. Gibbs energy barriers G_b (in kcal/mol) on H-M-DHKUST-1 and other MOFs reported in literature.

	Hydrogenation	**C-C coupling**	**β-H elimination**	**1-butene desorption**	**Ref.**
H-Co-DHKUST-1	0.9	19.3	10.4	8.4	This work
H-Ni-DHKUST-1	4.7	22.5	9.9	3.6	This work
H-Cu-DHKUST-1	18.4	22.7	28.5	7.0	This work
H-Ru-DHKUST-1	4.7	37.3	1.6	7.7	This work
H-Rh-DHKUST-1	5.5	39.6	0.2	17.9	This work
H-Pd-DHKUST-1	5.4	30.0	19.2	3.2	This work
MFU-4*l*(Ni)	10.7	22.0	17.3	–6.1	[36, 47]
Ni-NU-1000	3.7	13.7	9.6	5.7	[48]
Co-NU-1000	8.3	24.8	22.3	–4.0	[48]
Cu-NU-1000	2.3	20.9	23.8	–6.0	[48]
Pd-NU-1000	3.5	12.3	1.5	16.4	[48]

C-C coupling: After hydrogenation, intermediate **3** is formed with ethyl coordinated on H-M-DHKUST-1, thus vacant site is available and the second ethylene molecule is adsorbed. Upon the adsorption to form intermediate **4**, as shown in **Figure 4**, Gibbs energy changes marginally on 3d metal-based clusters H-Co- (1.5 kcal/mol), H-Ni- (1.5 kcal/mol) and H-Cu-DHKUST-1 (−1.2 kcal/mol), but significantly on 4d metal clusters H-Ru- (−17.3 kcal/mol), H-Rh- (–23.7 kcal/mol) and H-Pd-DHKUST-1 (−10.5 kcal/mol). Apparently, the dimeric metal atoms play a crucial role in the change of Gibbs energy. As shown in **Figure 6** for the optimized structures of intermediate **4**, the distances between the secondary metal and the H atom of ethyl are 1.82 and 1.76 Å on H-Ru- and H-Rh-DHKUST-1, respectively, which are shorter than those on the other four clusters. Moreover, the distances between the primary metal atom and the second adsorbed ethylene are also shorter on H-Ru- and H-Rh-DHKUST-1 (2.16 and 2.14 Å) compared to 2.61 ~ 2.76 Å on the other four clusters. These shorter distances of metal atom

with ethyl and second adsorbed ethylene stabilize intermediate **4** on H-Ru- and H-Rh-DHKUST-1, thus reducing Gibbs energy upon adsorption. In addition, Ru and Rh atoms are observed to have the lowest NBO charges of 0.321*e* and 0.369*e* upon second ethylene adsorption, as shown in **Tables S11-S12**, with triplet-to-quintet and triplet-to-closed shell singlet multiplicity transitions, respectively.

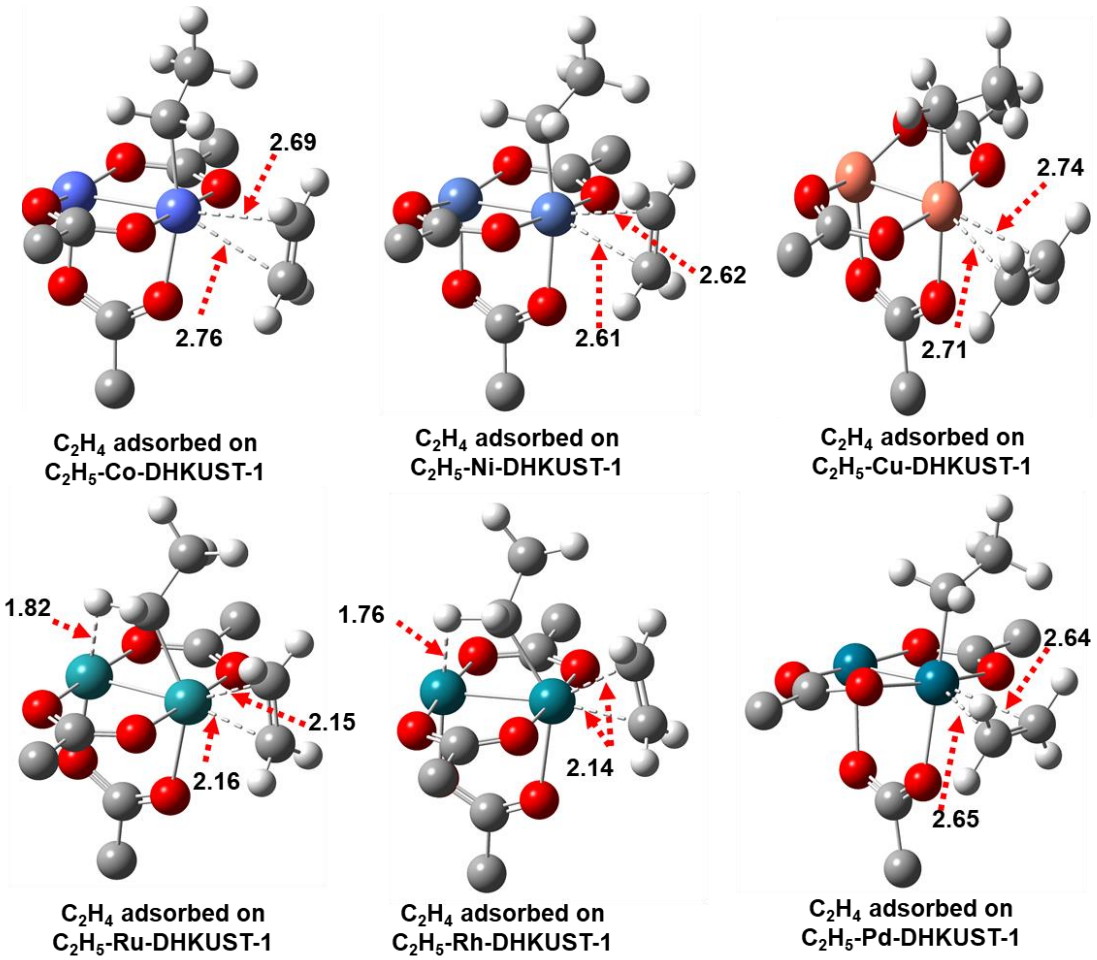


Figure 6. Optimized structures and key bond distances (in Å) of intermediate **4** for the adsorption of second ethylene molecule on ethyl-M-DHKUST-1. Carbon, oxygen and hydrogen atoms are in grey, red and white, respectively.

It is observed in **Figure 6** that the second adsorbed ethylene tends to align horizontally with the metal atoms on H-Cu- and H-Pd-DHKUST-1, and vertically with the metal atoms on the other four clusters. Geometrically, the vertically aligned ethylene is likely to couple with ethyl. In **Table 2**, the Gibbs energy barriers G_b for C-C coupling are 19.3, 22.5, 22.7 kcal/mol on 3d metal-based H-Co-, H-Ni- and H-Cu-DHKUST-1; on 4d metal-based clusters, the G_b are generally higher. Particularly, G_b on H-Ru- and H-Rh-DHKUST-1 are the highest of 37.3 and 39.6 kcal/mol among the six clusters. This is attributed to the most stable intermediate **4** on H-

Ru- and H-Rh-DHKUST-1, as discussed above. From the optimized structures of transition state **TS4-5** in **Figure S9**, we observe ethylene reorientation and C-C distance shortening upon C-C coupling. In addition, the M-M bonds are elongated from intermediate **4** to **TS4-5**, as listed in **Tables S8-S13**, from 2.44 to 2.61 Å on H-Co-DHKUST-1, 2.36 to 2.47 Å on H-Ni-DHKUST-1, 2.57 to 2.91 Å on H-Cu-DHKUST-1, 2.36 to 2.39 Å on H-Ru-DHKUST-1, 2.42 to 2.71 Å on H-Rh-DHKUST-1, and 2.58 to 2.62 Å on H-Pd-DHKUST-1.

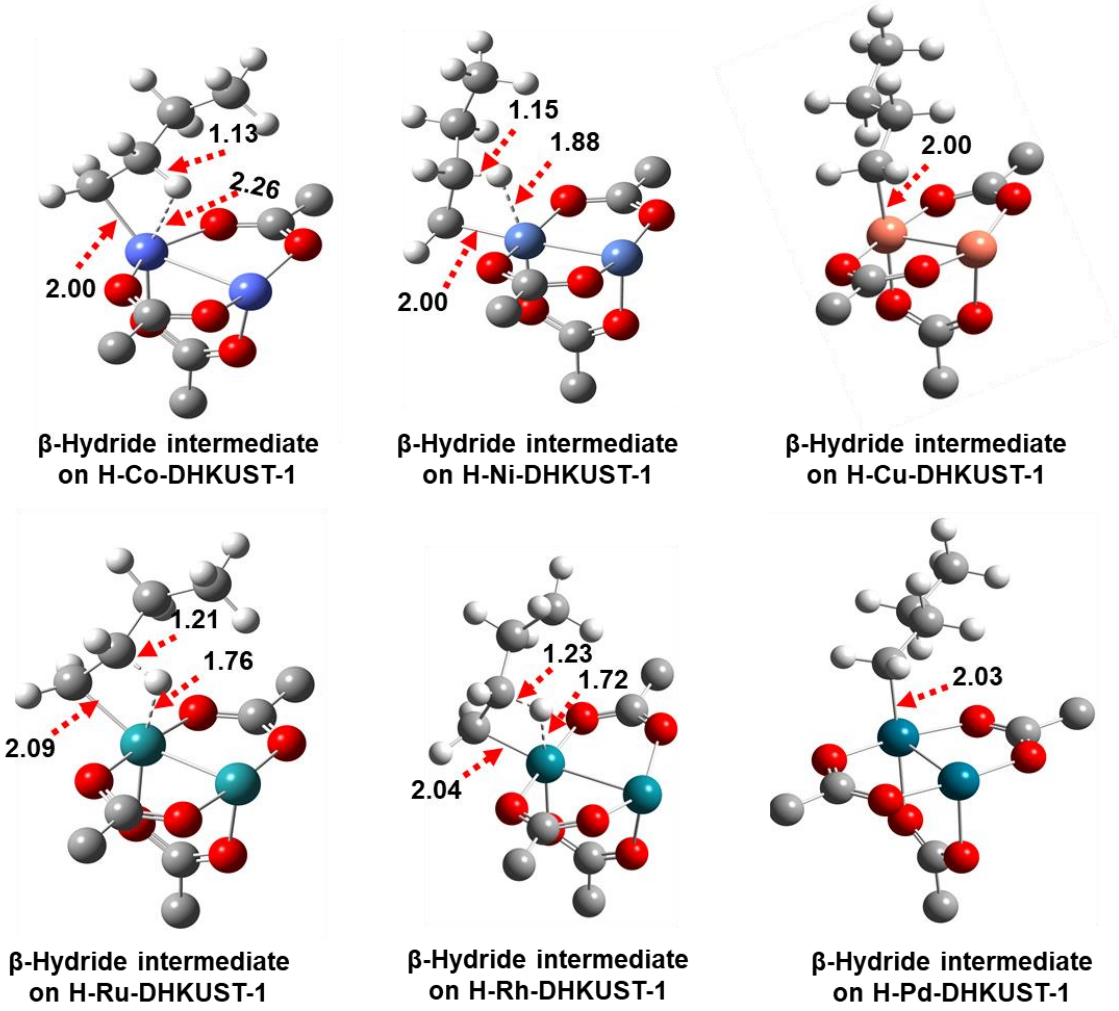


Figure 7. Optimized structures and key bond distances (in Å) of intermediate **6** for β-hydride elimination on H-M-DHKUST-1. Carbon, oxygen and hydrogen atoms are in grey, red and white, respectively.

β-hydride elimination: The third step is the elimination of hydride from β-C of butyl after intermediate **5** is structurally reoriented into intermediate **6**. The reorientation is exergonic on H-Co- (3.5 kcal/mol), H-Ni- (1.3 kcal/mol), and H-Cu- (1.5 kcal/mol), while endergonic on H-Ru-DHKUST-1 (–8.6 kcal/mol), H-Rh- (–6.1 kcal/mol) and H-Pd-DHKUST-1 (–10.3 kcal/mol). From **Figure 7** for the optimized structures of intermediate **6**, close contacts between

metals and the C−H bond of butyl (i.e., agostic arrangement) are observed on four clusters (H-Co-, H-Ni-, H-Ru- and H-Rh-DHKUST-1). Moreover, the β-C-hydride bonds on these clusters are found to be elongated compared to aliphatic C-H bond (1.10 Å). Usually, the longer the β-C-hydride bond, the easier is β-hydride elimination (BHE), and such a trend was observed on 2H-DHKUST-1.[21, 24] Therefore, facile BHE occurs on the four clusters with G_b of 10.4, 9.9, 1.6 and 0.2 kcal/mol, respectively (**Table 2**). This is consistent with experimental observation of high selectivity for 1-butene on defective Ru-HKUST-1.[24] Comparatively, there is no agostic arrangement on H-Cu- and H-Pd-DHKUST-1 at all the calculated multiplicities, giving high G_b of 28.5 and 19.2 kcal/mol, respectively. Interestingly, as shown in **Figure S10**, agostic arrangement is present in the transition state **TS6-7** on all the six clusters. Meanwhile, the β-C-hydride bonds become longer and the M-H bonds become shorter than the corresponding bonds in intermediate **6**. The high performance of BHE on H-Co-, H-Ni-, H-Ru-, and H-Rh-DHKUST-1 is accompanied with a considerable decrease in the NBO charges of main metals: Co (0.158*e*), Ni (0.393*e*), Ru (0.053*e*) and Rh (0.212*e*),) as listed in **Tables S8-S9** and **Tables S11-S12**. We should note that BHE is an essential step for ethylene dimerization, isomerization, or subsequent oligomerization of 1-butene, it is important to examine the ground-state structures of reacting species involved. In future study, we plan to further perform comprehensive calculations to explore the possibility of different reactions through competing pathways.

1-butene desorption: The last step is 1-butene desorption from H-M-DHKUST-1 involving the release of 1-butene from intermediate **7**. As shown in **Figure 8**, the distances between the C atom of 1-butene and the metal of cluster in intermediate **7** are comparatively longer than those in **TS6-7** (**Figure S10**). The desorption step is endergonic on all the clusters (**Figure 4**). As listed in **Table 2**, the G_b are 8.4, 3.6, 7.0, 7.7, 17.9, and 3.2 kcal/mol on H-Co-, H-Ni-, H-Cu-, H-Ru-, H-Rh- and H-Pd-DHKUST-1. The high G_b predicted on H-Rh-DHKUST-1 is associated with the short distance between 1-butene and Rh atom as seen in **Figure 8**. **Tables S8-S13** show that the adsorption of 1-butene causes a marked decrease in the NBO charges of the primary metal atoms on H-Co-, H-Ru- and H-Rh-DHKUST-1. Additionally, Ni and Cu clusters undergo a multiplicity transition, similar to the effect observed in ethylene adsorption and hydrogenation.

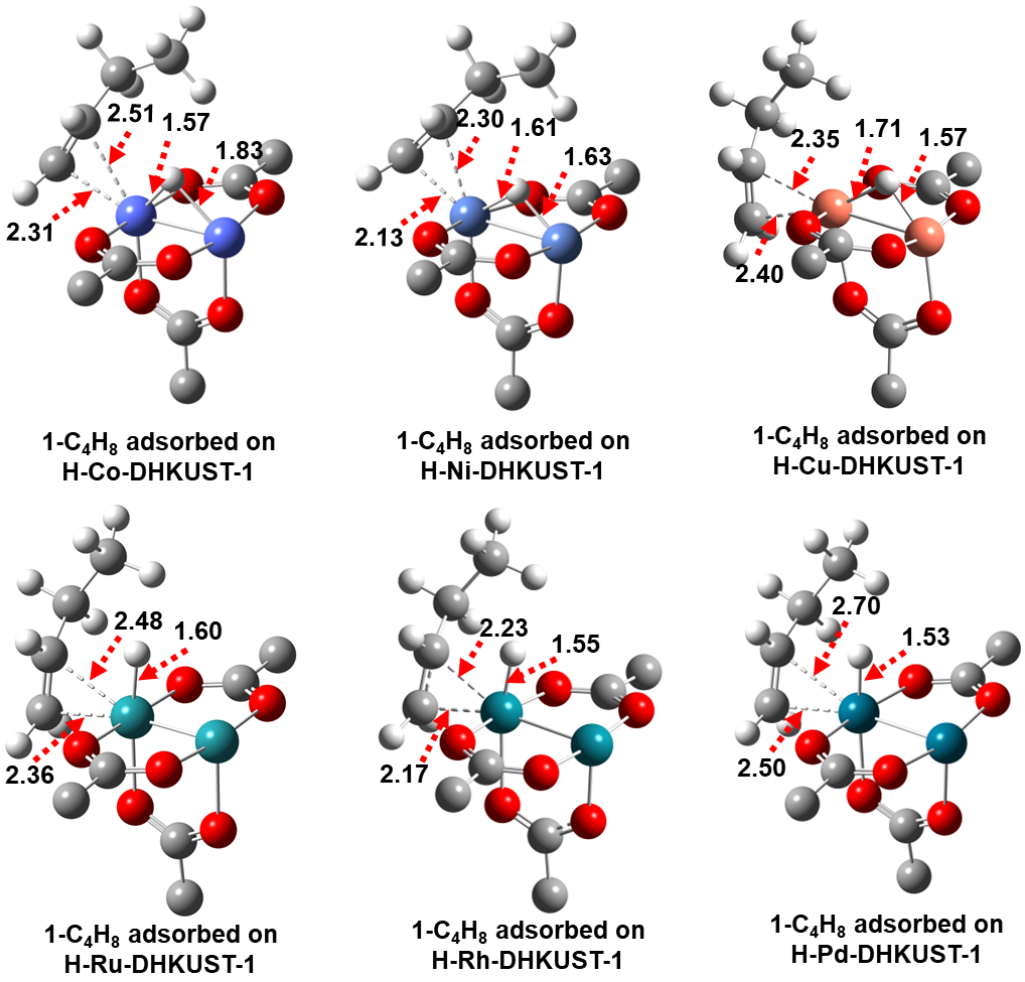


Figure 8. Optimized structures of intermediate **7** on H-M-DHKUST-1. Carbon, oxygen and hydrogen atoms are in grey, red and white, respectively.

By comparing the above four elementary steps (**Table 2**), we find that the G_b for C-C coupling is the highest on all the six clusters, except H-Cu-DHKUST-1 on which the G_b for BHE is the highest. This reveals that BHE is the rate-determining step in ethylene dimerization on H-Cu-DHKUST-1, but C-C coupling is on the other five clusters. Overall, H-Co- and H-Ni-DHKUST-1 are predicted to outperform the other four. It is also instructive to compare the catalytic performance of H-M-DHKUST-1 under this study with other MOF catalysts reported in the literature. As tabulated in **Table 2**, H-M-DHKUST-1, MFU-4*l*(Ni), Ni, Co, Cu and Pd-decorated NU-1000 exhibit similar magnitude of G_b (< 10 kcal/mol) for hydrogenation, however, H-Cu-DHKUST-1 (18.4 kcal/mol) is an exception to this trend. For C-C coupling, the G_b on H-M-DHKUST-1 are generally higher than MFU-4*l*(Ni) and metal-decorated NU-1000. Particularly, the G_b are 37.3, 39.6, 30.0 kcal/mol on the precious metal-based H-Ru-, H-Rh- and H-Pd-DHKUST-1. This reveals that H-M-DHKUST-1 clusters are less active for C-C

coupling; comparatively, Ni-NU-1000 and Pd-NU-1000 with square-planar Pd sites are more favoured with G_b of 13.7 and 12.3 kcal/mol, respectively. For BHE, H-Ru- and H-Rh-DHKUST-1 are predicted to have the lowest G_b of only 1.6 and 0.1 kcal/mol respectively, leading to facile formation of 1-butene. On Pd-NU-1000, G_b of 1.5 kcal/mol is also rather low due to agostic arrangement, in contrast to 17.1 kcal/mol on octahedral sites of H-Pd-DHKUST-1 without agostic arrangement.[40, 48] However, the desorption of 1-butene on H-Rh-DHKUST-1 and Pd-NU-1000 is impeded by high G_b (17.9 and 1.64 kcal/mol).

Ni-based catalysts have been extensively examined for ethylene dimerization. Square-planar configuration was revealed to be the stable structural environment on Ni-exchanged MFU-4*l* and Ni-supported NU-1000.[35, 47] The G_b on MFU-4*l*(Ni) were predicted to be 10.7, 22.0 and 17.3 kcal/mol for hydrogenation, C-C coupling and BHE,[36, 47] and lower G_b (3.7, 13.7 and 9.6 kcal/mol) were estimated on Ni-NU-1000.[48] Despite the difference in electronic environment, H-Ni-DHKUST-1 with octahedral site possesses similar G_b (4.7, 22.5 and 9.9 kcal/mol). The reason is the electron withdrawal by oxygen atoms in organic linkers facilitates BHE on H-Ni-DHKUST-1. Comparatively, H-Co-DHKUST-1 displays lower G_b (0.9, 19.3 and 10.4 kcal/mol) than Co-NU-1000 (8.3, 24.8 and 22.3 kcal/mol) for hydrogenation, C-C coupling and BHE, suggesting its better catalytic performance and the octahedral site of H-Co-DHKUST-1 is more effective than triagonal pyramidal site of Co-NU-1000. However, Cu-NU-1000 shows greater tendency for hydrogenation (2.3 kcal/mol) and facilitates 1-butene desorption (−6.0 kcal/mol) compared to H-Cu-DHKUST-1, which requires higher G_b for the same steps (18.4 and 7.0 kcal/mol).

3.3. Effects of multiplicity

As pointed out above, it is important to investigate the effects of multiplicity on catalytic properties. **Tables S14-S19** and **Figures S2-S7** compare the Gibbs energies at different multiplicities on H-M-DHKUST-1. Due to the binding and coordination of reacting species with catalyst, intersystem crossing (ISC) may occur and two energy surfaces at different multiplicities compete for the ground state.[47, 49-52] It is observed that the ground-state multiplicity on H-M-DHKUST-1 shows a decreasing trend upon moving through the same row of 3d transition metals. On H-Co-DHKUST-1, quintet and triplet are the dominant ground-state multiplicities in most intermediates and transitions states, except for septet in intermediate **5** (**Figure S2**). Triplet-singlet crossing is seen on H-Ni-DHKUST-1 (**Figure S3**), while singlet (open and closed shells) is the only ground-state multiplicity on H-Cu-DHKUST-1 (**Figure S4**). A similar trend exists on the 4d transition metal H-M-DHKUST-1. On H-Ru-DHKUST-

1, there is ISC between quintet and triplet, though quintet is more prevalent (**Figure S5**). On H-Rh-DHKUST-1, closed-shell singlet and triplet states compete with each other (**Figure S6**). However, triplet is the common ground-state multiplicity on H-Pd-DHKUST-1 with open-shell singlet existing only in intermediate **6** (**Figure S7**).

Ethylene dimerization is remarkably associated with the interplay between electronic configuration and structural environment of catalyst. A singlet-to-triplet ISC was reported on MFU-4*l*(Ni) from square-planar to tetrahedral for ethylene dimerization and oligomerization.[47] Similarly, ISC between triplet and singlet is also observed on H-Ni-DHKUST-1. As illustrated by **Figure S3**, triplet persists in most of the intermediates and transition states, but it switches to open-shell singlet in intermediates **2** and **7** upon the adsorption of ethylene and 1-butene, respectively. Compared to triplet, singlet exhibits lower Gibbs energy (0.9 kcal/mol in intermediate **2** and 1.7 kcal/mol in intermediate **7**). The reason is that H-Ni-DHKUST-1 with octahedral site requires 7-fold-like arrangement upon coordinating with ethylene molecule and 1-butene (**Figures 5** and **8**), thus adopting singlet as the ground state with bridged-like hydride. Such a configuration allows easy hydrogenation (with a low G_b of 4.7 kcal/mol), as well as facile 1-butene desorption (with a low G_b of 3.6 kcal/mol). In this context, it is helpful to understand the significance of ISC during ethylene adsorption and 1-butene desorption to practically tailor the catalytic performance toward ethylene dimerization.[47, 53]

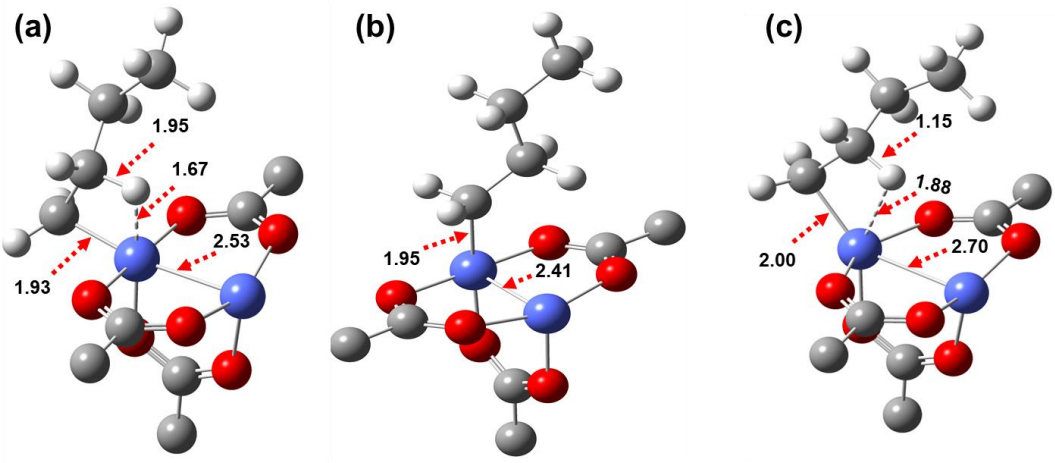


Figure 9. Intermediate **6** on H-Co-DHKUST-1 with different multiplicities (a) triplet, (b) quintet and (c) septet. Quintet displays the lowest Gibbs energy with non-agostic arrangement, while triplet and septet exhibit agostic arrangement with 10.4 and 4.0 kcal/mol higher Gibbs energy, respectively.

The electronic-structural intercorrelations at different multiplicities are also observed on other H-M-DHKUST-1 except for H-Cu-DHKUST-1. There is quintet-to-triplet crossing on H-Ru-DHKUST-1 (**Figures S2** and **S5**), while triplet-to-singlet crossing is seen on H-Rh- and H-Pd-DHKUST-1 (**Figures S6** and **S7**). Interestingly, certain structures are not fully attainable at all multiplicities. For instance, agostic arrangement of β-hydride intermediate **6** on H-Co-DHKUST-1 is not observed at quintet state; instead, a reoriented butyl-intermediate (**Figure 9b**) is formed. On the other hand, intermediate **6** is attainable with agostic arrangement at both triplet (**Figure 9a**) and septet states (**Figure 9c**). As shown in **Figure S2**, the quintet has a lower Gibbs energy (–39.8 kcal/mol) than triplet (–29.4 kcal/mol) and septet (–39.8 kcal/mol). Nevertheless, agostic arrangement is crucial for BHE, thus the septet structure essentially represents intermediate **6** on H-Co-DHKUST-1 and the G_b for BHE is thus 10.4 kcal/mol. Similarly, agostic arrangement is not observed to be feasible at singlet and triplet states on H-Cu-DHKUST-1 and H-Pd-DHKUST-1 (**Figures S11** and **S12**).

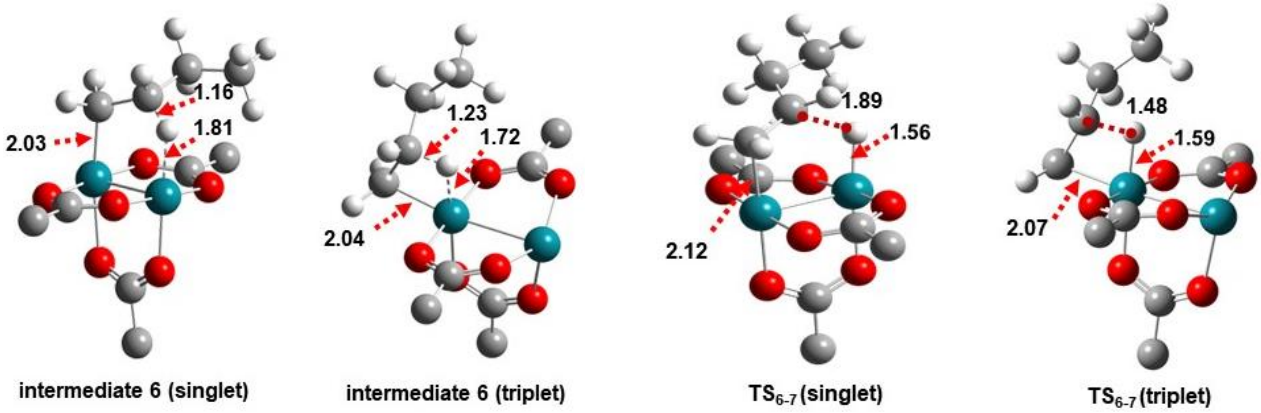


Figure 10. Intermediate **6** and transition state **TS6-7** on H-Rh-DHKUST-1 with closed-shell singlet and triplet states. Closed-shell singlet displays pentacyclic arrangement, while triplet exhibits agostic arrangement with 2.4 and 3.0 kcal/mol lower in Gibbs energy, respectively.

Figure 10 further highlights the role of multiplicity during BHE on H-Rh-DHKUST-1. The closed-shell singlet state is found to allow for pentacyclic stabilization of intermediate **6** and transition state **TS6-7** in a synergistic manner of both metal atoms. Comparatively, the triplet adopts agostic arrangement with 2.4 and 3.0 kcal/mol lower in Gibbs energy (**Figure S6**). With such a small energy difference, BHE could be sidestepped by other reaction pathways unless the secondary metal atom is fully saturated.[24] This observation underpins the importance of complete saturation of the secondary metal atom in dimeric metal catalysts for ethylene dimerization. Overall, ISC is revealed to be crucial to determine the reaction pathway. Nevertheless, the significance between difference multiplicities is not highly appreciable

among analogous geometries, because the energy difference is usually only within a few kilocalories. As shown on H-Pd-HKUST-1, the energy profiles of singlet and triplet states are nearly identical (**Figure S7**).

4. Conclusions

We have computationally designed metal hydrides on defective HKUST-1 (H-M-DHKUST-1 (M: Co, Ni, Cu, Ru, Rh and Pd) and investigate their catalytic performance for ethylene dimerization. Four elementary steps in the Cossse-Arlman route are considered including initiation, C-C coupling, β-hydride elimination, and 1-butene desorption. For each step, the Gibbs energy profiles are comprehensively calculated at all possible multiplicities. Interestingly, intersystem spin crossing is observed on the six H-M-DHKUST-1 clusters, revealing the importance of electronic-structural intercorrelations in ethylene dimerization. Compared to 3d metal (Co, Ni and Cu) based H-M-DHKUST-1, 4d metal (Ru, Rh and Pd) based are predicted to be less favorable in C-C coupling but more active in β-hydride elimination (BHE). Particularly, the Gibbs energy barriers are only 1.6 and 0.2 kcal/mol for BHE on H-Ru- and H-Rh-DHKUST-1, respectively. However, the energy barrier for 1-butene desorption is high of 17.9 kcal/mol on H-Rh-DHKUST-1 due to strong stability of adsorbed 1-butene. From the calculated results, the rate determining step is determined to be C-C coupling on H-Co-, H-Ni-, H-Ru-, H-Rh- and H-Pd-DHKUST-1 with Gibbs energy barriers of 19.3, 22.5, 37.3, 39.6 and 30.0 kcal/mol, respectively. The barriers on H-Ru- and H-Pd-DHKUST-1 are the highest due to the interference of the second metal atom. Nevertheless, BHE is the rate determining on H-Cu-DHKUST-1 with barrier of 28.5 kcal/mol, as a result of stabilization of non-agostic arrangement. Overall, H-Co- and H-Ni-DHKUST-1 are predicted to outperform the other four counterparts. This computational study provides not only microscopic insights into the catalytic activity and performance of bimetallic H-M-DHKUST-1, but also quantitative understanding of the effects of electronic configuration and structural environment of H-M-DHKUST-1 on ethylene dimerization. These bottom-up insights are useful to facilitate the rational design of defective MOF catalysts for important catalytic reactions.

Acknowledgments

We gratefully acknowledge the A*STAR LCER-FI project (LCERFI01-0033 U2102d2006), the Ministry of Education of Singapore and the National University of Singapore (C-261-000-207-532/C-261-000-777-532 and R-279-000-574-114) for financial support.

Supporting Information

Transition metals; stability and multiplicity tests; optimized M-M bond distances and NBO analysis; Gibbs energies at different multiplicities; frequencies and structures of transition states;; coordinates.

References

(1) Programme, U. N. E. *Global Chemicals Outlook II: From Legacies to Innovative Solutions: Implementing the 2030 Agenda for Sustainable Development*; 2019.

(2) Bender, M. An Overview of Industrial Processes for the Production of Olefins - C4 Hydrocarbons. *ChemBioEng Reviews* **2014**, *1* (4), 136-147. DOI: 10.1002/cben.201400016.

(3) Skupinska, J. Oligomerization of .alpha.-olefins to higher oligomers. *Chemical Reviews* **1991**, *91* (4), 613-648. DOI: 10.1021/cr00004a007.

(4) Dement'ev, K. I.; Sagaradze, A. D.; Kuznetsov, P. S.; Palankoev, T. A.; Maximov, A. L. Selective Production of Light Olefins from Fischer–Tropsch Synthetic Oil by Catalytic Cracking. *Industrial & Engineering Chemistry Research* **2020**, *59* (36), 15875-15883. DOI: 10.1021/acs.iecr.0c02753.

(5) McGuinness, D. S. Olefin Oligomerization via Metallacycles: Dimerization, Trimerization, Tetramerization, and Beyond. *Chemical Reviews* **2011**, *111* (3), 2321-2341. DOI: 10.1021/cr100217q.

(6) Agapie, T. Selective ethylene oligomerization: Recent advances in chromium catalysis and mechanistic investigations. *Coordination Chemistry Reviews* **2011**, *255* (7), 861-880. DOI: https://doi.org/10.1016/j.ccr.2010.11.035.

(7) Lallemand, M.; Finiels, A.; Fajula, F.; Hulea, V. Catalytic oligomerization of ethylene over Ni-containing dealuminated Y zeolites. *Applied Catalysis A: General* **2006**, *301* (2), 196-201. DOI: https://doi.org/10.1016/j.apcata.2005.12.019.

(8) Finiels, A.; Fajula, F.; Hulea, V. Nickel-based solid catalysts for ethylene oligomerization – a review. *Catalysis Science & Technology* **2014**, *4* (8), 2412-2426, 10.1039/C4CY00305E. DOI: 10.1039/C4CY00305E.

(9) Hulea, V.; Fajula, F. Ni-exchanged AlMCM-41—An efficient bifunctional catalyst for ethylene oligomerization. *Journal of Catalysis* **2004**, *225* (1), 213-222. DOI: https://doi.org/10.1016/j.jcat.2004.04.018.

(10) Furukawa, H.; Cordova, K. E.; O'Keeffe, M.; Yaghi, O. M. The Chemistry and Applications of Metal-Organic Frameworks. *Science* **2013**, *341*, 1230444. DOI: https://doi.org/10.1126/science.1230444.

(11) Fang, Z.; Bueken, B.; De Vos, D. E.; Fischer, R. A. Defect-Engineered Metal–Organic Frameworks. *Angewandte Chemie International Edition* **2015**, *54* (25), 7234-7254. DOI: https://doi.org/10.1002/anie.201411540.

(12) Nijem, N.; Fürsich, K.; Bluhm, H.; Leone, S. R.; Gilles, M. K. Ammonia adsorption and co-adsorption with water in HKUST-1: spectroscopic evidence for cooperative interactions. *The Journal of Physical Chemistry C* **2015**, *119* (44), 24781-24788.

(13) Zhang, W.; Kauer, M.; Guo, P.; Kunze, S.; Cwik, S.; Muhler, M.; Wang, Y.; Epp, K.; Kieslich, G.; Fischer, R. A. Impact of synthesis parameters on the formation of defects in HKUST‐1. *European Journal of Inorganic Chemistry* **2017**, *2017* (5), 925-931.

(14) Ren, J.; Rogers, D. E. C.; Segakweng, T.; Langmi, H. W.; North, B. C.; Mathe, M.; Bessarabov, D. Thermal treatment induced transition from $Zn_3(OH)_2(BDC)_2$ (MOF-69c) to $Zn_4O(BDC)_3$ (MOF-5). *International Journal of Materials Research* **2014**, *105* (1), 89-93. DOI: 10.3139/146.110994.

(15) Borges, D. D.; Devautour‐Vinot, S.; Jobic, H.; Ollivier, J.; Nouar, F.; Semino, R.; Devic, T.; Serre, C.; Paesani, F.; Maurin, G. Proton Transport in a Highly Conductive Porous Zirconium‐Based Metal‐Organic Framework: Molecular Insight. *Angewandte Chemie International Edition* **2016**, *55* (12), 3919-3924.

(16) Vermoortele, F.; Bueken, B.; Le Bars, G.; Van de Voorde, B.; Vandichel, M.; Houthoofd, K.; Vimont, A.; Daturi, M.; Waroquier, M.; Van Speybroeck, V. Synthesis modulation as a tool to increase the catalytic activity of metal–organic frameworks: the unique case of UiO-66 (Zr). *Journal of the American Chemical Society* **2013**, *135* (31), 11465-11468.

(17) Liu, Y.; Klet, R. C.; Hupp, J. T.; Farha, O. Probing the correlations between the defects in metal–organic frameworks and their catalytic activity by an epoxide ring-opening reaction. *Chemical Communications* **2016**, *52* (50), 7806-7809.

(18) Ren, J.; Ledwaba, M.; Musyoka, N. M.; Langmi, H. W.; Mathe, M.; Liao, S.; Pang, W. Structural defects in metal–organic frameworks (MOFs): Formation, detection and control towards practices of interests. *Coordination Chemistry Reviews* **2017**, *349*, 169-197.

(19) Zhang, C.-L.; Zhou, T.; Li, Y.-Q.; Lu, X.; Guan, Y.-B.; Cao, Y.-C.; Cao, G.-P. Microenvironment Modulation of Metal–Organic Frameworks (MOFs) for Coordination Olefin

Oligomerization and (co)Polymerization. *Small* **2023**, *n/a* (n/a), 2205898. DOI: https://doi.org/10.1002/smll.202205898.

(20) Goetjen, T. A.; Liu, J.; Wu, Y.; Sui, J.; Zhang, X.; Hupp, J. T.; Farha, O. K. Metal–organic framework (MOF) materials as polymerization catalysts: a review and recent advances. *Chemical Communications* **2020**, *56* (72), 10409-10418. DOI: 10.1039/d0cc03790g.

(21) Heinz, W. R.; Kratky, T.; Drees, M.; Wimmer, A.; Tomanec, O.; Günther, S.; Schuster, M.; Fischer, R. A. Mixed precious-group metal–organic frameworks: a case study of the HKUST-1 analogue [RuxRh3−x(BTC)2]. *Dalton Transactions* **2019**, *48* (32), 12031-12039, 10.1039/C9DT01198F. DOI: 10.1039/C9DT01198F.

(22) Kozachuk, O.; Luz, I.; Llabres i Xamena, F. X.; Noei, H.; Kauer, M.; Albada, H. B.; Bloch, E. D.; Marler, B.; Wang, Y.; Muhler, M.; et al. Multifunctional, defect‐engineered metal‐organic frameworks with ruthenium centers: sorption and catalytic properties. *Angewandte Chemie International Edition* **2014**, *53* (27), 7058-7062.

(23) Zhang, W.; Kauer, M.; Halbherr, O.; Epp, K.; Guo, P.; Gonzalez, M. I.; Xiao, D. J.; Wiktor, C.; Liabrés i Xamena, F. X.; Wöll, C.; et al. Ruthenium Metal–Organic Frameworks with Different Defect Types: Influence on Porosity, Sorption, and Catalytic Properties. *Chemistry – A European Journal* **2016**, *22* (40), 14297-14307, https://doi.org/10.1002/chem.201602641. DOI: https://doi.org/10.1002/chem.201602641 (acccessed 2022/10/18).

(24) Agirrezabal-Telleria, I.; Luz, I.; Ortuño, M. A.; Oregui-Bengoechea, M.; Gandarias, I.; López, N.; Lail, M. A.; Soukri, M. Gas reactions under intrapore condensation regime within tailored metal–organic framework catalysts. *Nature Communications* **2019**, *10* (1), 2076. DOI: 10.1038/s41467-019-10013-6.

(25) Arlman, E.; Cossee, P. Ziegler-Natta catalysis III. Stereospecific polymerization of propene with the catalyst system TiCl3 · AlEt3. *Journal of Catalysis* **1964**, *3* (1), 99-104.

(26) Yeh, B.; Chheda, S.; Prinslow, S. D.; Hoffman, A. S.; Hong, J.; Perez-Aguilar, J. E.; Bare, S. R.; Lu, C. C.; Gagliardi, L.; Bhan, A. Structure and Site Evolution of Framework Ni Species in MIL-127 MOFs for Propylene Oligomerization Catalysis. *Journal of the American Chemical Society* **2023**, *145* (6), 3408-3418. DOI: 10.1021/jacs.2c10551.

(27) Löbbert, L.; Chheda, S.; Zheng, J.; Khetrapal, N.; Schmid, J.; Zhao, R.; Gaggioli, C. A.; Camaioni, D. M.; Bermejo-Deval, R.; Gutiérrez, O. Y.; et al. Influence of 1-Butene Adsorption on the Dimerization Activity of Single Metal Cations on UiO-66 Nodes. *Journal of the American Chemical Society* **2023**, *145* (2), 1407-1422. DOI: 10.1021/jacs.2c12192.

(28) Chui, S. S.-Y.; Lo, S. M.-F.; Charmant, J. P. H.; Orpen, A. G.; Williams, I. D. A Chemically Functionalizable Nanoporous Material [Cu₃(TMA)₂(H₂O)₃]_n. *Science* **1999**, *283* (5405), 1148-1150. DOI: doi:10.1126/science.283.5405.1148.

(29) Zhao, Y.; Truhlar, D. G. A new local density functional for main-group thermochemistry, transition metal bonding, thermochemical kinetics, and noncovalent interactions. *The Journal of Chemical Physics* **2006**, *125* (19), 194101. DOI: 10.1063/1.2370993 (acccessed 2018/11/05).

(30) Weigend, F.; Ahlrichs, R. Balanced basis sets of split valence, triple zeta valence and quadruple zeta valence quality for H to Rn: Design and assessment of accuracy. *Physical Chemistry Chemical Physics* **2005**, *7* (18), 3297-3305, 10.1039/B508541A. DOI: 10.1039/B508541A.

(31) Shen, L.; Yang, S.-W.; Xiang, S.; Liu, T.; Zhao, B.; Ng, M.-F.; Göettlicher, J. r.; Yi, J.; Li, S.; Wang, L. Origin of long-range ferromagnetic ordering in metal–organic frameworks with antiferromagnetic dimeric-Cu (II) building units. *Journal of the American Chemical Society* **2012**, *134* (41), 17286-17290.

(32) Hendon, C. H.; Walsh, A. Chemical principles underpinning the performance of the metal–organic framework HKUST-1. *Chemical Science* **2015**, *6* (7), 3674-3683, 10.1039/C5SC01489A. DOI: 10.1039/C5SC01489A.

(33) Francisco, M. A. S.; Fantuzzi, F.; Cardozo, T. M.; Esteves, P. M.; Engels, B.; Oliveira, R. R. Taming the Antiferromagnetic Beast: Computational Design of Ultrashort Mn−Mn Bonds Stabilized by N-Heterocyclic Carbenes. *Chemistry – A European Journal* **2021**, *27* (47), 12126-12136. DOI: https://doi.org/10.1002/chem.202101116.

(34) Frisch, M. J.; Trucks, G. W.; Schlegel, H. B.; Scuseria, G. E.; Robb, M. A.; Cheeseman, J. R.; Scalmani, G.; Barone, V.; Petersson, G. A.; Nakatsuji, H.; Li, X.; Caricato, M.; Marenich, A. V.; Bloino, J.; Janesko, B. G.; Gomperts, R.; Mennucci, B.; Hratchian, H. P.; Ortiz, J. V.; Izmaylov, A. F.; Sonnenberg, J. L.; Williams; Ding, F.; Lipparini, F.; Egidi, F.; Goings, J.; Peng, B.; Petrone, A.; Henderson, T.; Ranasinghe, D.; Zakrzewski, V. G.; Gao, J.; Rega, N.; Zheng, G.; Liang, W.; Hada, M.; Ehara, M.; Toyota, K.; Fukuda, R.; Hasegawa, J.; Ishida, M.; Nakajima, T.; Honda, Y.; Kitao, O.; Nakai, H.; Vreven, T.; Throssell, K.; Montgomery Jr., J. A.; Peralta, J. E.; Ogliaro, F.; Bearpark, M. J.; Heyd, J. J.; Brothers, E. N.; Kudin, K. N.; Staroverov, V. N.; Keith, T. A.; Kobayashi, R.; Normand, J.; Raghavachari, K.; Rendell, A. P.; Burant, J. C.; Iyengar, S. S.; Tomasi, J.; Cossi, M.; Millam, J. M.; Klene, M.; Adamo, C.; Cammi, R.; Ochterski, J. W.; Martin, R. L.; Morokuma, K.; Farkas, O.; Foresman, J. B.; Fox, D. J. *Gaussian 16 Revision A.03*, Wallingford, CT, 2016.

(35) Bernales, V.; League, A. B.; Li, Z.; Schweitzer, N. M.; Peters, A. W.; Carlson, R. K.; Hupp, J. T.; Cramer, C. J.; Farha, O. K.; Gagliardi, L. Computationally Guided Discovery of a Catalytic Cobalt-Decorated Metal–Organic Framework for Ethylene Dimerization. *The Journal of Physical Chemistry C* **2016**, *120* (41), 23576-23583. DOI: 10.1021/acs.jpcc.6b07362.

(36) Ortega, D. E.; Matute, R. A. Influence of linkers on the Kuratowski-type secondary building unit in nickel single-site MOFs for ethylene oligomerization catalysis: a computational study. *Catalysis Science & Technology* **2021**, *11* (7), 2422-2432, 10.1039/D0CY02137G. DOI: 10.1039/D0CY02137G.

(37) Ye, J.; Gagliardi, L.; Cramer, C. J.; Truhlar, D. G. Computational screening of MOF-supported transition metal catalysts for activity and selectivity in ethylene dimerization. *J. Cat.* **2018**, *360*, 160-167. DOI: https://doi.org/10.1016/j.jcat.2017.12.007.

(38) Metzger, E. D.; Brozek, C. K.; Comito, R. J.; Dincă, M. Selective Dimerization of Ethylene to 1-Butene with a Porous Catalyst. *ACS Central Science* **2016**, *2* (3), 148-153. DOI: 10.1021/acscentsci.6b00012.

(39) Castiñeira Reis, M.; López, C. S.; Kraka, E.; Cremer, D.; Faza, O. N. Rational Design in Catalysis: A Mechanistic Study of β-Hydride Eliminations in Gold(I) and Gold(III) Complexes Based on Features of the Reaction Valley. *Inorganic Chemistry* **2016**, *55* (17), 8636-8645. DOI: 10.1021/acs.inorgchem.6b01188.

(40) Theofanis, P. L.; Goddard, W. A., III. Understanding β-Hydride Eliminations from Heteroatom Functional Groups. *Organometallics* **2011**, *30* (18), 4941-4948. DOI: 10.1021/om200542w.

(41) Debnath, T.; Ash, T.; Banu, T.; Das, A. K. Investigation of agostic interaction through NBO analysis and its impact on β-hydride elimination and dehydrogenation: a DFT approach. *Theoretical Chemistry Accounts* **2016**, *135* (7), 175. DOI: 10.1007/s00214-016-1939-0.

(42) Weinhold, F.; Landis, C. R. *Valency and bonding: a natural bond orbital donor-acceptor perspective*; Cambridge University Press, 2005.

(43) Pirillo, J.; Hijikata, Y. Trans Influence across a Metal–Metal Bond of a Paddle-Wheel Unit on Interaction with Gases in a Metal–Organic Framework. *Inorganic Chemistry* **2020**, *59* (2), 1193-1203. DOI: 10.1021/acs.inorgchem.9b02911.

(44) Hrdina, R. Dirhodium(II,II) Paddlewheel Complexes. *European Journal of Inorganic Chemistry* **2021**, *2021* (6), 501-528. DOI: https://doi.org/10.1002/ejic.202000955.

(45) Raghavan, A.; Ren, T. Bisaryl Diruthenium(III) Paddlewheel Complexes: Synthesis and Characterization. *Organometallics* **2019**, *38* (19), 3888-3896. DOI: 10.1021/acs.organomet.9b00555.

(46) Wang, C.; Li, G.; Guo, H. Ethylene Dimerization Performance of NiBTCs Synthesized Using Different Solvents. *Catalysts* **2023**, *13* (3), 640.

(47) Mancuso, J. L.; Gaggioli, C. A.; Gagliardi, L.; Hendon, C. H. Singlet-to-Triplet Spin Transitions Facilitate Selective 1-Butene Formation during Ethylene Dimerization in Ni(II)-MFU-4l. *The Journal of Physical Chemistry C* **2021**, *125* (40), 22036-22043. DOI: 10.1021/acs.jpcc.1c07658.

(48) Ye, J.; Gagliardi, L.; Cramer, C. J.; Truhlar, D. G. Computational screening of MOF-supported transition metal catalysts for activity and selectivity in ethylene dimerization. *Journal of Catalysis* **2018**, *360*, 160-167. DOI: https://doi.org/10.1016/j.jcat.2017.12.007.

(49) Farcaș, A.-A.; Bende, A. Improving the Light-Induced Spin Transition Efficiency in Ni(II)-Based Macrocyclic-Ligand Complexes. *Molecules* **2019**, *24* (23), 4249.

(50) Brandenburg, H.; Krahmer, J.; Fischer, K.; Schwager, B.; Flöser, B.; Näther, C.; Tuczek, F. Coordination-Induced Spin-State Switching with Nickel(II) salpn Complexes: Electronic versus Steric Effects and Influence of Intermolecular Interactions. *European Journal of Inorganic Chemistry* **2018**, *2018* (5), 576-585. DOI: https://doi.org/10.1002/ejic.201701281.

(51) Homma, Y.; Ishida, T. A New S = 0 ⇄ S = 2 "Spin-Crossover" Scenario Found in a Nickel(II) Bis(nitroxide) System. *Chemistry of Materials* **2018**, *30* (6), 1835-1838. DOI: 10.1021/acs.chemmater.7b05357.

(52) Dommaschk, M.; Schütt, C.; Venkataramani, S.; Jana, U.; Näther, C.; Sönnichsen, F. D.; Herges, R. Rational design of a room temperature molecular spin switch. The light-driven coordination induced spin state switch (LD-CISSS) approach. *Dalton Trans.* **2014**, *43* (46), 17395-17405. DOI: 10.1039/c4dt03048f.

(53) Comito, R. J.; Metzger, E. D.; Wu, Z.; Zhang, G.; Hendon, C. H.; Miller, J. T.; Dincă, M. Selective Dimerization of Propylene with Ni-MFU-4l. *Organometallics* **2017**, *36* (9), 1681-1683. DOI: 10.1021/acs.organomet.7b00178.